Myelodysplastic Syndrome associated TET2 mutations affect NK cell function and genome methylation

Maxime Boy, Valeria Bisio, Lin-Pierre Zhao, Fabien Guidez, Bérénice Schell, Emilie Lereclus, Guylaine Henry, Juliette Villemonteix, Fernando Rodrigues-Lima, Katia Gagne, et al.

Peer review information: *Nature Communications* thanks Ivo Touw, Jörn Walter and the other, anonymous, reviewer(s) for their contribution to the peer review of this work.

Myelodysplastic Syndrome associated *TET2* mutations affect NK cell function and genome methylation

Maxime Boy[1-3,#], Valeria Bisio[1-3,#], Lin-Pierre Zhao[1-3], Fabien Guidez[2,4], Bérénice Schell[1-3], Emilie Lereclus[1-3], Guylaine Henry[5], Juliette Villemonteix[5], Fernando Rodrigues-lima, Katia Gagne[7-10], Christelle Retiere[7-10], Lise Larcher[2,11], Rathana Kim[2,11], Emmanuelle Clappier[2,11], Marie Sebert[2,12,13], Arsène Mekinian[14,15], Olivier Fain[14,15], Anne Caignard[1,2], Marion Espeli[1-3], Karl Balabanian[1-3], Antoine Toubert[1,2,5], Pierre Fenaux[2,12,13], Lionel Ades[2,12,13], and Nicolas Dulphy[1-3,5]*

[1]Université Paris Cité, Institut de Recherche Saint Louis, EMiLy, INSERM UMR_S1160, F-75010 Paris, France;

[2]Institut Carnot OPALE, Institut de Recherche Saint-Louis, Hôpital Saint-Louis, F-75010 Paris, France;

[3]CNRS, GDR3697 "Microenvironment of tumor niches", Micronit, F-75010 Paris, France;

[4]Université Paris Cité, Institut de Recherche Saint Louis INSERM UMR_S1131, F-75010 Paris, France;

[5]Laboratoire d'Immunologie et d'Histocompatibilité, Assistance Publique des Hôpitaux de Paris (AP-HP), Hôpital Saint-Louis, F-75010 Paris, France;

[6]Universite Paris Cité, Sorbonne Paris Cite, Unité BFA, CNRS UMR 8251, 75013, Paris, France;

[7]Etablissement Français du Sang, Centre Pays de la Loire, F-44011 Nantes, France;

[8]Université de Nantes, INSERM UMR1307, CNRS UMR 6075, CRCI[2]NA team 12, F-44000 Nantes, France;

[9]LabEx IGO « Immunotherapy, Graft, Oncology » F-44000 Nantes, France;

[10]LabEx Transplantex, Université de Strasbourg, 67000 Strasbourg, France;

[11]Laboratoire d'Hématologie, Hôpital Saint-Louis, AP-HP, F-75010 Paris, France;

[12]Department d'Hématologie Sénior, Hôpital Saint-Louis, AP-HP, F-75010 Paris, France;

[13]Université Paris Cité, Institut de Recherche Saint Louis INSERM UMR_944, F-75010 Paris, France;

[14]Service de Medecine Interne, Hôpital Saint-Antoine, AP-HP, F-75012 Paris, France;

[15]Sorbonne Université, Departement Hospitalo-Universitaire Inflammation-Immunopathologie-Biotherapie, Hôpital de la Pitié-Salpêtrière, F-75013 Paris, France

[#]These authors contributed equally to this work: Maxime BOY and Valeria BISIO.

*Corresponding author. Email: nicolas.dulphy@u-paris.fr

Abstract:

Myelodysplastic syndromes (MDS) are clonal hematopoietic disorders, representing high risk of progression to acute myeloid leukaemia, and frequently associated to somatic mutations, notably in the epigenetic regulator *TET2*. Natural Killer (NK) cells play a role in the anti-leukemic immune response via their cytolytic activity.

Here we show that patients with MDS clones harbouring mutations in the *TET2* gene are characterised by phenotypic defects in their circulating NK cells. Remarkably, NK cells and MDS clones from the same patient share the *TET2* genotype, and the NK cells are characterised by increased methylation of genomic DNA and reduced expression of Killer Immunoglobulin-like receptors (KIR), perforin, and TNF-α. *In vitro* inhibition of TET2 in NK cells of healthy donors reduces their cytotoxicity, supporting its critical role in NK cell function. Conversely, NK cells from patients treated with azacytidine (#NCT02985190; https://clinicaltrials.gov/) show increased KIR and cytolytic protein expression, and IFN-γ production. Altogether, our findings show that, in addition to their oncogenic consequences in the myeloid cell subsets, *TET2* mutations contribute to repressing NK-cell function in MDS patients.

Introduction:

Myelodysplastic Syndromes (MDS) are clonal myeloid malignancies characterized by ineffective hematopoiesis and bone marrow (BM) failure leading to blood cytopenias and a high risk of transformation to Acute Myeloid Leukaemia (AML)[1]. MDS patients with high risk of AML progression ("high-risk MDS" according to international prognostic scoring system) are treated with hypomethylating agents (HMA) including azacitidine (AZA) and decitabine (DAC) which can increase overall survival and reduce AML progression[2,3]. Mutations in *TET2* and *IDH1/2* genes, involved in the epigenetic regulation of gene transcription, are common genetic alterations found in MDS[1]. Whereas *TET2* encodes for a methylcytosine dioxygenase catalyzing the oxidation of the methyl group of 5-methycytosine (5mC) to 5-hydroxymethylcytosine (5-hmC), the isocitrate dehydrogenases (IDH) 1 and 2 control the production of α-ketoglutarate (αKG), a metabolite required for TET2 activity[4]. Most *TET2* mutations described are loss of function, and generally mutually exclusive with *IDH1/2* mutations. By contrast, *IDH1/2* mutations in MDS lead to a new enzymatic activity that generates 2-hydroxyglutarate (2HG) in place of αKG and inhibits TET2 activity[5]. Therefore, *TET2* and *IDH1/2* mutations lead to hypermethylation of the genomic DNA in myeloid cells[6]. MDS patients carrying mutations in *TET2* are more likely to respond to HMA treatment[7], but mechanisms of action of HMA on MDS cells are still unclear and could involve BM microenvironment, including immune (lymphocytes, myeloid-derived suppressive cells)[8] and non-immune partners (mesenchymal stromal cells)[9].

Natural Killer (NK) lymphocytes are key players in the anti-leukemic response. NK cell targets malignant cells by direct cytotoxicity through release of perforin, granzymes, engagement of death receptors, or secreting cytokines like IFN-γ and TNF-α[10,11]. Their function is regulated by a balance between inhibitory (KIR, NKG2A) and activating (NKp30, NKp46, DNAM-1, NKG2D) receptors. We and others have shown defects in NK cell phenotype and function in AML and MDS patients[12,13,14,15], but mechanisms leading to deficient NK cells are still unclear. Moreover, whether the enhanced sensitivity to HMA treatment of MDS patients with *TET2/IDH*^{MUT} relies on the restoration of NK-cell activity is unknown.

In this study, we show MDS *TET2/IDH* mutations are carried by NK cells and associated with defects in phenotype and function. Those perturbations rely on genome-wide hypermethylation of DNA, leading to the reduced expression of key molecules for NK cell function. Finally, HMA treatment normalizes the expression of NK cell related genes *in vitro* as well as *in vivo.* Altogether, our results established that TET2 regulates NK-cell biology, and suggest that HMA treatments in *TET2/IDH* mutated patients could also be beneficial by restoring the functionality of NK cells.

Results

MDS/CMML patients with TET2/IDH mutations display a distinct NK cell phenotype

Blood NK cells from 33 MDS/CMML patients (myelodysplastic syndromes and chronic myelomonoytic leukaemia, respectively, Supplementary Data 1) and 23 HD were phenotyped by flow-cytometry. Surface expression of maturation markers (CD69, CD57, KLRG1), activating (NKp30, NKp46, DNAM-1, NKG2D) and inhibitory (CD96, KIR2D, CD85j) receptors was investigated (Supplementary Table 1). Small perturbations were observed on circulating NK cells of MDS/CMML individuals compared with HD in the expression of some activating (DNAM-1, NKp46) and inhibitory (CD96) receptors. Surprisingly, an almost 2-fold reduction of the killer immunoglobulin-like receptors (KIR) expression was found on MDS patients NK cells compared to HD (31.2% and 54.8% respectively, $p<0.01$, Supplementary Table 1).

We asked whether patients with mutations affecting DNA methylation (i.e., mutations in *TET2*, *IDH1* or *IDH2*) could exhibit specific NK-cell phenotype (Fig. 1, Supplementary Table 1). Interestingly, a deep loss in the expression of KIRs with 2 Ig-like extracellular domains (KIR2D) was observed in patients with *TET2/IDH* mutations compared to *TET2/IDH*^{WT} on blood (n= 19 vs 13, median 11.9% vs. 56.5%, $p<0.001$, Fig. 1A) and BM NK cells (n= 7 vs 12, median 24.2% vs 45.9% $p<0.05$, Fig. 1B). In parallel, the inhibitory receptor NKG2A was significantly increased on peripheral NK cells in *TET2/IDH*^{MUT} patients compared to *TET2/IDH*^{WT} (n=15 vs. 11, 86.3% vs. 78.7%, p=0.025, Fig. 1A, Supplementary Table 2), underlying the balance between KIRs and NKG2A expression[16]. Of note, the KIR-positive T-cell subset was not affected by the *TET2/IDH* mutational status in patients (Supplementary Fig. 1). Importantly, censuring the few patients treated with either drugs to stimulate the erythro-thrombopoiesis (EPO n=4 out of 63 patients, TPO n=1) or immunomodulating molecules (lenalidomide n=4, glucocorticoid n=4) did not modify our observations demonstrating that treatments were not at the origin of the decrease in KIR expression (Supplementary Fig. 2).

KIRs are encoded in a 15 genes locus with high variability in genes content across individuals[17]. To investigate if *TET2/IDH* mutations could differentially affect *KIR* genes expression, the KIR locus was genotyped for 22 MDS/CMML patients, and KIR surface expression was analyzed for genes highly present with KIR2DL1, KIR2DL2/DL3, and KIR3DL1/DL2 specific mAbs (Fig. 1C-D, Supplementary Fig. 3 and Table 3). We confirmed a specific reduction of KIR2DL1 (3.6% vs. 14.1%, $p<0.01$) and KIR2DL2/DL3 (10.3% vs. 29.1%, $p<0.01$) on NK cells of *TET2/IDH*^{MUT} patients compared to WT (n=15 vs. n=11 respectively) (Fig. 1C-D, Supplementary Table 2). By contrast, KIR3DL1/DL2 expression was not significantly modified by the *TET2/IDH* mutation status (Fig. 1D), despite the strong reduction observed in some patients (Fig. 1C-D).

We next quantified perforin and granzyme B expression in NK cells of MDS/CMML patients as surrogate markers of NK-cell cytolytic capacity. We observed a reduced percentage of perforin-positive NK cells in *TET2/IDH*^{MUT} patients ($p<0.05$), whereas granzyme B expression was not affected (Fig. 1E). This loss of intracellular perforin was correlated with reduced KIR (KIR2D and KIR3DL1/DS1) expression at the NK-cell surface in *TET2/IDH*^{MUT} patients ($r=0.65$, $p=0.001$; Supplementary Fig. 4). Indeed, the loss of perforin expression was mainly observed in KIR$^-$ NK cells whereas KIR$^+$ NK-cells were not affected (Supplementary Fig. 5**)**, suggesting a co-regulation of KIR and perforin expressions.

Then, we reasoned that TET2 function may be the main parameter modifying the NK cell phenotype. Therefore, we analyzed the performance of KIR2D expression as a classifier of patients with or without *TET2* mutations by calculating a receiver operation characteristic (ROC) curve using KIR2D expression on circulating NK cells in *TET2/IDH*^{WT} (n=19) and *TET2*^{MUT} (n=17) patients. A maximum area under the curve (AUC) equal to 0.89 predicted that a threshold of 25% of KIR2D$^+$ NK cells allowed classifying mutated and not-mutated patients with a specificity of 95% and a sensitivity of 77% ($p<0.0001$, Fig. 1F). Studying KIR2D expression separately in *TET2*^{MUT} and *IDH1*/2^{MUT} patients, we observed that 4 out of 5 patients mutated for either *IDH1* or *IDH2* showed a comparable decrease of KIR2D expression than *TET2*^{MUT} individuals (Fig. 1G). This observation confirmed that *IDH1/2* mutations could phenocopy *TET2* mutations at least when considering NK cell phenotype.

Altogether, our results unraveled a strong relationship between the presence of mutations in *TET2* and *IDH1/2* genes in MDS/CMML patients and the alterations in NK-cell phenotype. To gain further insights into the molecular mechanisms accounting for this loss of NK cell function, we focused our study on *TET2* mutated patients, excluding the *IDH* mutated patients from our cohort, and interrogated whether NK and MDS cells could share *TET2* mutations.

TET2 mutations observed in MDS/CMML patients at diagnosis can be found in blood NK-cells

All MDS/CMML patients recruited in this study were analyzed at diagnosis of the disease for the presence of somatic mutations in 80 genes usually found mutated in myeloid malignancies (Supplementary Table 4). As expected, $TET2^{MUT}$ and $TET2/IDH^{WT}$ patients could show mutations in additional genes frequently observed in MDS/CMML[1], including *SRSF2* (29% and 3% respectively), *SF3B1* (18% and 20% respectively) or *ASXL1* (18% and 17% respectively) (Supplementary Fig. 6 and Supplementary Table 5). Of note, $TET2^{MUT}$ patients presented a mean of 2 mutations in *TET2* (range 1-4 mutations).

Thus, we analyzed whether MDS-associated mutations were present in NK cells. PBMC of 10 MDS patients diagnosed with mutations in *TET2* among other genes were sorted for NK cells. Nine out 10 patients showed some mutations in NK cells shared with the blood or BM white mononuclear cell (WMC) samples at diagnosis, including in *TET2* and other genes (Supplementary Table 6). The variant allele frequencies (VAF) for *TET2* mutations were not significantly different in NK cells (median=11%, range 0 – 54%) compared to WMC (median=32%, range 2 - 49%, Fig. 2A). By contrast, consistent with their unchanged phenotype previously observed, MDS-associated mutations were rarely found in T cells (Supplementary Table 6, Supplementary Fig. 7A), and with a VAF below 7% when present (Fig. 2A). Importantly, whereas 7 patients presented a strict concordance in the mutation profiles between analyses

on WMC and NK cells (Fig. 2B and Supplementary Table 6), 3 patients (MUT19, MUT22, MUT31) showed mutations in NK cells unobserved in WMC (Fig. 2B).

Furthermore, we observed a strong correlation between the expression of KIR2D receptor and the VAF of *TET2* mutations in NK cells (Fig. 2C, R^2=0.88, p<0.0001). In the 10 patients analyzed by NGS, those with a percentage of $KIR2D^+$ NK-cells below 25% showed a *TET2* mutation VAF higher than 20% in the WMC at diagnosis and higher or equal to 34% in the NK-cell subset. To confirm this observation, we selected 5 patients with sufficient amount of $KIR2D^+$ and $KIR2D^-$ NK cells and performed a NGS analysis on cells sorted according to the expression of the KIR2D and KIR3DL1/DL2 (hereafter designed has KIR^+ or KIR^- NK cells). Importantly, 4 out of 5 patients showed a high percentage of $KIR2D^+$ cells, superior to the threshold of 25% we have calculated previously (Fig. 1F). As expected, patients showed higher $TET2^{MUT}$ VAF in the KIR^- (median= 18.2%, range 6.1 – 42.1%) than the KIR^+ cells (median= 5%, range 0 – 48%, p<0.01, Fig. 2D, Supplementary Fig. 7B). In addition, KIR^- NK cell subset showed *TET2* mutations leading to non-functional TET2 proteins in all patients tested. In detail, patients MUT08, MUT19 and MUT23 presented frameshift mutations, leading to premature stop-codon, with VAFs ranging from 22% to 37% in KIR^- cells, as compared to a range from 2% to 15% in the KIR^+ cells. Patients MUT24 and MUT32 showed missense mutations in the TET2 catalytic domain, with VAFs ranging from 11% to 39% in the KIR^- cells as compared to 1% to 7% in the KIR^+ cells. Moreover, two patients (MUT19 and MUT23) showed a shared nonsense mutation at position 548 only present in the KIR^- NK cells. Moreover, mutations in other genes were also enriched in the KIR^- population (Supplementary Table 6). Altogether, these observations suggested that *TET2* mutations can be found in NK cells and are related to reduced KIR expression in $TET2^{MUT}$ MDS/CMML patients.

TET2 directly binds to and regulates KIR locus expression in NK cells

To evaluate the role of TET2 in regulating KIR expression, we first analyzed the type and the positioning of the *TET2* mutations found in MDS/CMML patients with a reduced percentage of KIR^+ NK cells

(below 25 %) at diagnosis (Fig. 3A). This analysis revealed that all but one patient showed either nonsense or frameshift mutations leading to a premature stop-codon and the absence of a functional TET2 protein, extending the observation made in KIR^- NK cells (Supplementary Table 6). The only exception was the patient MUT30 who presented a missense mutation p.R1261H (c.G3782A substitution). This mutation has already been described in the catalogue of somatic mutations in cancer (COSMIC) database[18] with a functional consequence prediction (Functional Analysis through Hidden Markov Models FATHMM) score equal to 0.99[19], forerunning a highly significant functional impact on the TET2 protein.

Therefore, we asked whether the inhibition of the enzymatic function of TET2 in NK cells could also lead to a significant reduction of the KIR2D proteins expression. We treated NK cells from healthy individuals with dimethyloxalyl glycine (DMOG), an α-ketoglutarate (α-KG) analog which inhibits α-KG-dependent enzymes including TET2[20]. In line with our results in *TET2*^{MUT} MDS patients, TET2 inhibition in DMOG treatment significantly reduced the percentage of $KIR2D^+$ NK cells ($p<0.001$, Fig. 3B), suggesting a role for TET2 in modulating the KIR expression on NK cells or the $KIR2D^+$ subset proliferation.

We then sought to determine whether TET2 had a direct impact on *KIR* genes expression. We performed chromatin immunoprecipitation (ChIP) followed by real time qPCR analysis on sorted NK cells from control PBMC with a TET2-specific monoclonal antibody (mAb), and evaluated the presence of the proximal promoter regions of *KIR2DL1* and *KIR2DL2/3* genes. We also tested TET2 binding site onto a predicted *cis*-regulatory element (CRE) localized upstream of the KIR locus (chr19:54,688,519-54.702.287)[21]. We found that tested KIR promoters and CRE sequences were enriched in TET2-specific ChIP fragments (Fig. 3C).

To substantiate the role of TET2 in driving KIR expression, we generated a luciferase reporter vector containing 210 (-147; +63) nucleotides of the predicted KIR2DL1 promoter associated with TET2 ChIP assay experiment. Co-transfection of this reporter with a TET2 overexpression vector into HEK293T cell line is associated with an increase of luciferase activity increased by 2.3-fold compared to the empty vector (Fig. 3D). To corroborate this data, the TET2 expressing Jurkat lymphoid cell line was transfected

with the KIR2DL1-luciferase reporter vector and then treated with ascorbic acid (L-AA), a catalyst of the TET2 hydroxylation activity of 5-methylcytosine in DNA and an already-known enhancer of the *KIR* locus demethylation[22,23]. We observed a significant increase of the luciferase signal by 2-fold in the treated condition compared to control, demonstrating that L-AA enhanced TET2 binding and activity onto the *KIR* promoter sequence (Fig. 3E).

Based on these observations, we anticipated that NK cells with low KIR expression and carrying *TET2* mutations could show perturbations in the methylation profile of the *KIR* locus. Therefore, we performed reduced representation bisulfite sequencing (RRBS) analysis on NK-cells sorted from $TET2^{WT}$ and $TET2^{MUT}$ MDS/CMML patients (n=1 and n=4 respectively, Fig. 3F-H) to assess their DNA methylation pattern. Three $TET2^{MUT}$ MDS/CMML patients were chosen based on a KIR2D expression on NK cells below 25%, and a *TET2* mutation VAF superior to 40% in the cell bulk at diagnosis ($TET2^{MUT}$ KIR^{LOW} patients: MUT22, MUT27, MUT33). One $TET2^{MUT}$ patient chosen because of a KIR2D expression on NK cells at 90% ($TET2^{MUT}$ KIR^{HIGH} patient: MUT14) and one $TET2^{WT}$ patient ($TET2^{WT}$ KIR^{HIGH} patient: WT13) were used as controls.

The analysis of the CpG islands in the CRE sequence and the *KIR2DL1* gene showed increased methylation in the three $TET2^{MUT}$ KIR^{LOW} patients compared to the $TET2^{MUT}$ KIR^{HIGH} and the $TET2^{WT}$ ones (Fig. 3G-H).

Altogether, these findings demonstrate the targeting of the *KIR* locus by TET2 and strongly suggest that loss of TET2 leads to the hypermethylation of the *KIR* locus in NK cells.

TET2 mutations lead to hypermethylation of key genes for cytotoxicity and cytokine release by NK cell

The analysis of DNA methylation in TET2-deficient mouse models showed widespread DNA hypermethylation, including in enhancer elements[24]. RRBS analyses of NK cells from $TET2^{MUT}$ KIR^{LOW} MDS/CMML patients confirmed that genomic DNA was more methylated in NK cells with a high VAF

of TET2^{MUT} and a reduced KIR2D cell surface expression compared to TET2^{WT} NK cells (Fig. 4A). We then asked whether *TET2* mutations in NK cells could interfere with the methylation and expression of genes relevant for NK cell function. RRBS analyses of NK cells from *TET2^{MUT}* KIR^{LOW} MDS/CMML patients showed a significant hypermethylation compared to KIR^{HIGH} patients with 11,594 hypermethylated CpG sites among the 15,827 differentially methylated sites (methylation difference ≥ 20%, $p \leq 0.05$) (Fig. 4B, upper panel, Supplementary Data 2). Among the 97 genes found hypermethylated in *TET2*^{MUT}KIR^{LOW} patients compared to KIR^{HIGH} patients (Fig. 4B, lower panel, Supplementary Data 3), methylation of *TYROBP* (coding for DAP12) and *TNF* was predicted to significantly inhibit the NK cell mediated cytotoxicity pathway as defined by the KEGG database (p<0.05, KEGG pathway hsa04650)[25]. Reports suggested variations in methylation by TET2 of the CpG loci according to their position regarding the gene body and the respective regulatory elements[24,26,27]. We analyzed the percentage of 5hmC in the gene bodies and 10kb upstream or downstream on the whole genome[26]. Then, mean of methylation has been calculated for genes involved in pathways of interest for NK cell biology. Percentage of 5hmC trends up in *TET2*^{MUT}KIR^{LOW} NK cells compared to KIR^{HIGH} samples in coding and flanking regions of genes implicated in the cytokine-cytokine receptor interactions (KEGG pathway reference hsa04060), the JAK-STAT signalling pathway (hsa04630), the TNF signalling pathway (hsa04668) and the NK cell mediated cytotoxicity (hsa04650) (Fig. 4C), indicating a decrease of these cell functions. Interestingly, the increase of methylation affected the gene bodies as well as their flanking regions, suggesting a differential role for TET2 in NK cells as compared to myeloid cells in which TET2 mainly regulates enhancers[24,27].

We then looked at the methylation of *IFNG*, *TNF* and *PRF1*, three genes determinant in NK cell anti-leukemic activity[28]. RRBS analysis showed hypermethylated CpG islands in the three loci in the *TET2^{MUT}*KIR^{LOW} patients compared to *TET2^{MUT}*KIR^{HIGH} or the *TET2^{WT}* patients, suggesting a reduced transcription of these genes (Fig. 5A).

To evaluate the functional relevance of DNA methylation in controlling the regulatory regions of these genes, a luciferase reporter assay was performed in the HEK293T cell line (Fig. 5B). Regions of interest,

showing differences in their methylation profile between *TET2*^{MUT}KIR^{LOW} and *TET2*^{MUT}KIR^{HIGH} NK cells, were cloned into a CpG-free vector upstream of the luciferase gene, without minimal promoter to determine the functional activity of the promoter. The constructs were then methylated *in vitro* specifically onto the insert sequences. Methylation resulted in significant decreased luciferase activity compared to the unmodified construct, suggesting that the promoter function of the region of interest is dampened upon DNA methylation (Fig. 5B). In parallel, the decreased expression of *TNF* and *INFG* in presence of *TET2* mutations was confirmed by qRT-PCR in KIR2D^{-} NK cell sorted from *TET2/IDH*^{WT} and *TET2*^{MUT} patients (Fig. 5C).

Altogether, these results showed that key molecules for NK-cell function were under the control of the TET2 demethylation pathway, and that their transcription was reduced in *TET2*^{MUT} NK cells.

Consequently, we asked whether TET2 inhibition could impair NK cell function. NK cells from HD were treated *in vitro* with DMOG and then co-cultured with the K562 cell line. As expected, K562 killing by DMOG-treated NK-cells was significantly reduced demonstrating that the NK-cell cytotoxicity pathway was, at least in part, under the control of TET2 ($p<0.05$, Fig. 5D).

Hypomethylating agents rescue KIR expression on MDS NK cells

To evaluate whether demethylation could restore KIR expression on NK cells, PBMC from *TET2*^{MUT} patients were cultured *in vitro* in presence of IL-2 and with or without AZA or DAC for 5 days. Then, KIR2D expression on NK cells was assessed by flow cytometry (Fig. 6A). Whereas AZA showed only a trend, DAC significantly restored the KIR expression on treated NK cells ($p=0.07$ and $p<0.001$ respectively). Further, L-AA was used either alone or in combination with DAC to treat PBMC of *TET2*^{MUT} MDS/CMML patients. L-AA associated with DAC significantly increased KIR expression on NK cells compared with DAC alone ($p<0.05$). Of note, NK cells from HD and TET2^{WT} patients also increased KIR expression in response to HMA with or without AA (Supplementary Fig.8).

To confirm *in vivo* our observations, NK cells from MDS patients recruited in the clinical trial NCT02985190 were analyzed for their capacity to produce IFN-γ and to restore their phenotype, before and after 3 or 6 cycles of treatment with AZA. NCT02985190 clinical trial is a phase II study of efficacy and tolerance of AZA in MDS patients with concomitant systemic auto-immune and inflammatory disorders (SAID), for which the primary outcome measure was the overall response rate of MDS and SAID[29]. Functional experiments showed an increase in the production of INF-γ by NK cells stimulated *in vitro* by a mixture of PMA and ionomycin in patients after 3 cycles of treatment with AZA (n=6, Fig. 6B). Moreover, KIR2D, perforin and granzyme B expressions, quantified by flow-cytometry, were significantly increased in this group of patients after 6 cycles of treatment (n=9, Fig.6C). Importantly, despite the absence of significance due to the small number of patients, this effect of AZA on NK cell phenotype and function was similar in $TET2^{WT}$ and $TET2^{MUT}$ patients.

Taken as a whole, these findings showed that demethylation mediated by TET2 is pivotal in regulating NK cell biology, including the expression of KIR and functional proteins, and, more importantly, that treatment by HMA could normalize the hypermethylated profile harboured by NK cells in MDS patients.

Discussion

In this work, we described the epigenetic, phenotypic, and functional consequences of *TET2* mutations for NK cells in MDS patients. We could demonstrate that mutations observed in MDS cancer cells, including in *TET2* and *IDH1/2* genes, are also generally observed in NK cells. Consequently, *TET2* mutations in NK cells are associated with perturbations in methylation of the genomic DNA inducing a reduced expression of KIRs, locus on which TET2 directly binds, and of other key molecules for NK cell function including perforin and TNF-α. The reduced KIR expression and cytotoxicity of NK cells of healthy donors after TET2 inhibition confirmed its requirement for an efficient physiological NK cell function. Finally, NK cell phenotype can be restored *in vitro* and *in vivo* after treatment with ascorbic acid and HMA.

The fact that NK cell defects observed in MDS can be partly due to the oncogenic mutations at the origin of the disease could suggest that both events (i.e. mutations in MDS cells and NK cells) may synergize to sustain the emergence of myeloid malignancies. Abnormalities in NK cell phenotype and function could reduce the antitumor immuno-surveillance efficacy and allow the survival of potential pre-leukemic progenitors. Notably, NK-cell perturbations in MDS patients including reduction of activating NK receptors, such as NKp30, DNAM-1 and NKG2D, and impaired cytotoxicity, have already been reported[12,15,30]. KIR genotype has also been associated with clinical outcome[31]. Our data suggest that these observations should be reinterpreted based on patient mutation profiles, especially for mutations associated with *TET2* or *IDH1/2* genes. In line with this comment, dissecting the specific role of TET2 in NK cells by contrast to other mutated genes commonly found in MDS or clonal hematopoiesis will require further investigations, which could be decisive in our comprehension of the disease and its treatments. Whether NK-cell function could be associated to a particular mutation landscape may have important consequences in developing NK-cell-based immunotherapeutic intervention. In that context, using autologous NK cells or attempting to rescue NK cell function in MDS patients may be impeded. Combining such therapeutic strategies with the use of HMA could provide a relevant option.

Loss-of-function somatic mutations in *TET2* are strongly associated with haematological malignancies, including myeloid, T- and B-cell malignancies and chronic lymphoproliferative disorders of NK cells (CLPD-NK)[32,33,34]. Germline mutations in *TET2* have been also associated with lymphoma[35,36]. Here, we found that *TET2* mutation in NK cells from MDS patients, with or without additional mutated genes, does not seem to affect NK cell from the oncogenic point of view (i.e. NK cells were not leukemic) but alters their phenotype and function. This raises the question of the requirement of other mutated genes, in addition to TET2, in order to induce malignant hemopathies and how these mutation profiles can be specific to lymphoid or myeloid malignancies.

Intriguingly, we noticed that TET2 mutations in NK cells trended to increase methylation together on the gene body and its flanking regions, at least for genes involved in NK cell function. TET2 has been reported as preferentially targeting regulatory enhancers in hematopoietic and myeloid cells, notably to facilitate the recruitment of transcription factors[24,27]. However, gene bodies and other genomic regions can be also, although in a less efficient manner, targeted by TET2[24]. In addition, our results could suggest that key genes for NK cell function, including *KIR* and *PRF1*, are regulated in a coordinated manner by TET2 and more generally DNA methylation. If it is confirmed, this hypothesis would point out TET2 as a master regulator in NK cell development and education. It remains to be investigated whether and how genomic DNA methylation by TET2 is differentially regulated in NK cells, compared to myeloid subsets, due to differences in chromatin modification and accessibility or in the timing of TET2 expression during NK-cell lymphopoiesis.

From the mechanistic point of view, our results are reminiscent of the work by Wu *et al* describing a role for the ascorbic acid in promoting KIR locus demethylation through the mobilization of Runx3, TET2 and TET3[22]. Interestingly, it has been recently shown that $TET2^{KO}$ HSC treated with ascorbic acid could increase the 5hmC levels suggesting a role for TET proteins other than TET2 in this rescuing[26]. Herein, we showed that the addition of ascorbic acid onto NK cells allow the restoration of KIR expression. Altogether, these data support the hypothesis that TET3 could compensate for TET2 mutations in NK cells after treatment with ascorbic acid.

Clonal hematopoiesis (CH) is frequently presented as a precursor state for haematological malignancies, upstream of a continuum including MDS and then AML[37]. Arends *et al* recently demonstrated that *TET2* mutations observed in individuals with CH could be found not only in myeloid lineage but also in B- and NK-cell[38]. Our results support the finding that CH infuses into the complete tree of the hematopoiesis, including lymphopoiesis, and could also participate to a reduced NK cell immunity in elderly. It remains to discover the mechanisms by which *TET2* mutations alter the production of new lymphocytes in the elderly without significantly reducing the lymphocyte number, and with which consequences for the immune response. High-throughput experimental strategies, including multiomics approaches combining RNAseq and ATACseq at the single cell level, applied not only to patients' samples but also to TET2-edited HSC[26] or iPSCs[36], may help to solve this question.

Altogether, our findings showed that TET2 is a key epigenetic regulator of NK-cells, and that *TET2* mutations associated with MDS can alter their phenotype and function. In that context, HMA treatments could normalize the hypermethylated profile harboured by NK cells in MDS patients, and may participate to the emergence of a NK cell-mediated anti-tumour immunosurveillance.

Methods

Patient cohorts and Samples

The first cohort was composed of 20 sternal bone marrow (BM) aspiration and 58 peripheral blood mononuclear cell (PBMC) samples that were collected from 63 MDS/CMML patients. Patients' samples were obtained with written informed consent in the Haematology Departments of the Saint Louis Hospital, Paris, France (Supplementary Data 1 and Table 7). MDS and CMML diseases were defined according to the World Health Organization 2016 criteria[39], and classified according to the Revised International Prognostic Scoring System (IPSS-R)[40]. Low-Risk (LR) disease was defined as IPSS-R very-low, low or intermediate whereas High-Risk (HR) disease designated as IPSS-R high and very-high. Disease evolution was assessed according to 2006 International Working Group criteria[41]. Among the 63 patients recruited, a few received treatments consisting in either Darbepoietin (EPO, n=4) or Eltrombopag (TPO, n=1) without obvious effect on immune cells, or the immunomodulating drugs Lenalidomid (n=4) or the glucocorticoid Prednisone (n=4). The second cohort was composed by MDS patients recruited in the clinical trial #NCT02985190 (sponsored by Groupe Francophone des Myélodysplasies [GFM]) and repeatedly treated with azacitidine at 75mg/m²/j subcutaneously daily for 7 days every 4 weeks[29] (Supplementary Table 8). In addition, PBMC samples from 23 healthy individuals (HD) were collected through the EFS (Etablissement Français du Sang) (median age = 46 [27-66]). The study was approved by the Ethical Board Ile-de-France X and conducted in accordance with Helsinki's declaration. Recruited patients gave their written informed consent for participating.

PBMCs were purified from BM and blood samples by using a ficoll-based gradient density method [13], and stored in liquid nitrogen to be further analysed.

Patient KIR genotyping

Generic *KIR* typing was performed using a *KIR* multiplex PCR-SSP method as previously described[42]. The presence or absence of *KIR2DL1*, *2DL2*, *2DL3*, *2DL5*, *3DL1*, *2DS1*, *2DS2*, *2DS3*, *2DS4/1D*, *2DS5*

and *3DS1* genes were assigned. *KIR* genotypes were determined based on the presence or the absence of activating KIR. Thus, an AA *KIR* haplotype was defined by the presence of only *KIR2DS4* or its deleted variant (1D) as activating *KIR* gene, and a B+ (AB, BB) *KIR* haplotype by the presence of several activating KIR genes. Centromeric (AA, AB, BB) and telomeric (AA, AB, BB) *KIR* motifs were defined considering *KIR2DL2/3/S2* and *KIR3DL1/S1/2DS1/2DS4* genes for centromeric and telomeric motifs respectively[43] (Supplementary Table 3).

Cell lines

HEK293T and Jurkat cells lines (ATCC) were maintained either with DMEM or RPMI1640 medium containing 10% of FBS, penicillin/streptomycin antibiotics and L-glutamine.

For the measurement of target lysis, K562 cells were first cultured overnight in RPMI1640 without phenol red (Gibco) enriched with 10% FBS, non-essential amino acids (NEAA, Gibco), L-glutamine (Life Technologies) and Sodium Pyruvate (Eurobio). Prior killing assay, K562 cells were diluted at 1.10^6/mL in culture medium supplemented with 2.5mM Probenecid (Invitrogen) and stained with calcein-AM (Invitrogen) for 30min. Then, excess of calcein was washed out.

For *in vitro* cell treatment, PBMCs were resuspended in RPMI 1640 supplemented with 10% Human Serum (EFS, Etablissement Français du Sang), 1% Penicillin-Streptomycin (Dutscher), L-glutamine (Life Technologies), Sodium Pyruvate (EuroBio) and HEPES (EuroBio).

Flow Cytometry Analysis

Frozen sternal BM aspiration and PBMCs were stained for 30min on ice[13], with the fixable viability dye eFluor 506 and monoclonal antibodies (mAb) listed in Supplementary Table 9. Of note, mAb used in this work to detect KIR molecules on cell surface were able to identify KIR2DL1, KIR2DL2/DL3, KIR2DL4, KIR3DL1/DL2, KIR3DL1/DS1, KIR2DL5 and KIR2DS4 molecules. Cells were fixed in PBS with 2% of paraformaldehyde (PFA), acquired on a BD Fortessa X20 (flow cytometry core facility of Saint Louis

Research Institute, Paris, France) (Supplementary Fig. 9). For intracellular staining, Foxp3 Transcription factor buffer set (eBioscence 00-5523-00) was used and data were acquired on a BD Canto II or Cytek Aurora flow cytometer. Data was analyzed using FlowJo v10.7 software or Cytek SpectroFlo v3.0.3.

NK and T-cells isolation for Mutational Analysis and reduced representation bisulfite sequencing (RRBS)

After thawing, PBMCs were first labeled in PBS 30min at 4°C with the fixable viability dye eFluor 506 (eBioscience) and then stained with antibodies specific for surface markers to distinguish NK cell subsets (at the whole or based on the surface expression of KIR2D and KIR3DL1/DL2 molecules) and T-cells, and directly sorted using BD Aria III system (Supplementary Table 9 and Supplementary Fig. 10). Dry pellets have been stored after cells sorting for DNA extraction. DNA was purified according to manufacturer (DNeasy KIT, Qiagen) and quantify by Qubit (Thermofisher) for NGS and RRBS studies. Of notes, clinical evaluation of MDS mutations were performed in the haematology laboratory, in St-Louis hospital, Paris, on WMC obtained using gradient density separation on either BM or blood samples. A panel of 80 genes commonly analyzed in myeloid malignancies (Supplementary Table 4) was examined using next-generation sequencing on an Illumina platform (Illumina, San Diego, CA, USA). Libraries were prepared from 200 ng of DNA using a custom probes panel for capture of all coding sequences (SureSelectXT Target Enrichment System, Agilent, Santa Clara, CA, USA). Sequencing data were analyzed for variant calling using an in-house pipeline. High-probability pathogenic mutations were retained based on the available databases for SNPs, somatic mutations in cancer, prediction algorithm and frequencies of variant reads. Overall, a mean coverage of 851 reads/amplicon was achieved allowing reliable detection of low burden mutations. Lolliplot has been realized using the St Jude protein paint software available online at (https://proteinpaint.stjude.org/) (Fig. 3A)[44]. Major domains of TET2 protein were determined based on the work by Hu et al[45]. The mutational landscape was established using

cBioPortal Cancer Genomics Portal OncoPrinter software available online at (https://www.cbioportal.org/) (**Supplementary Fig. 4**).

RRBS was performed by Diagenode (Seraing, Belium) on dry samples of NK- and T-cell sorted from 5 MDS patients according to the manufacturer procedure. RRBS data are available on the Gene Expression Omnibus platform under the accession code GSE183020 (https://www.ncbi.nlm.nih.gov/geo/query/acc.cgi?&acc=GSE183020). 100ng of purified genomic DNA were used, including pre-RRBS quality control, enzymatic digestion and bisulfite conversion. Sequencing was performed in paired-end mode 50bp (PE50), quality control of sequencing reads was performed using FastQC, and reads alignment against human reference genome hg38/GRCh38 using Bismark v0.20.0 (available at https://www.bioinformatics.babraham.ac.uk/projects/bismark/) according to Diagenode protocol. Differential gene and site methylation analyses were performed by Genoplice Technology (Paris Biotech Santé, Paris, France). To assess the frequency of methylated CpG sites across all genes of a pathway of interest, gene lists were extracted from KEGG pathway website[25]. The position of each CpG site was calculated relatively to the transcript start and end positions as follows:

$$CG_{relativeposition} = \frac{CG_{position} - transcript\ start}{transcript\ end\ - transvript\ start}$$

Considering 10kb upstream and downstream sites. Next, frequency of methylation was calculated and aggregated across all genes of a given pathway for each sample.

Of note, all sequencing data were analysed using the human reference genome hg38/GRCh38.

Chromatin Immuno-Precipitation (ChIP)-qPCR assay

ChIP assay was performed with the Active Motif magnetic kit following the manufactory protocol. Briefly, after sonication the sheared chromatin was incubated overnight with TET2 (Diagenode, C15410255), control H3 (Abcam, AB1791) and H3K18 (Abcam, AB1191) specific mAb and the isotype control (Diagenode, C15410206). ChIP-enriched DNA was analyzed by qPCR with SYBR Green Master Mix (Thermofisher). Primers are listed in Supplementary Table 10.

Transfection and Luciferase assay

HEK293T cell lines (ATCC) were transfected by polyethylenimine (PEI, Sigma) following previous publication[46].

The plasmid pcDNA3-TET2 overexpressing the full-length mouse TET2 gene as the empty pcDNA3 vector were obtained from Addgene (Plasmid #60939 and #45346). All constructs have been verified by DNA sequencing.

One region of the predicted *KIR2DL1* promoter (KIRprom -147+60, Supplementary Fig. 11) was cloned in the pT109-tkLUC plasmid. 0.6µg promoter vector together with the 2.7µg TET2 plasmids were co-transfected in HEK293T cells with 0.06µg of pRL-CMV Vector (#E2261 Promega) in presence of PEI solution.

In parallel, Jurkat cells (ATCC) were transfected with 0.26µg of the KIR promoter plasmid and 0.026µg of pRL-CMV vector by Nucleofactor Kit V (Lonza). Jurkat transfected cells were then cultured at 1.10^6/mL and treated with 500µg of L-ascorbic acid (L-AA, Sigma) for 16h before analysis[47]. The luciferase activity was measured after 24h according to manufacturer's instructions (Dual-Luciferase Reporter Assay, Promega).

To investigate the role of the methylation in controlling the functional NK role, putative promoter regions, differentially methylated between KIR^{HIGH} and KIR^{LOW}, were cloned into pCpGfree basic vector (Invivogen) for testing promoter activity. To determine the effect of methylation on the activity of the region, *in vitro* methylation of the constructs was performed with M.SssI (NEB). 0.6µg promoter vector, "native" (unmethylated) or *in vitro* methylated, were co-transfected with 0.06µg of pRL-CMV Vector (#E2261 Promega) in presence of PEI solution. After 24h the Lucia and Firefly read-out was generated with a CLARIOstar^{Plus} (BMG LABTECH).

Microfluidic Multiplex qPCR

Multiplex qPCR analysis (Biomark, Fluidigm) was performed on 100 cells. NK cell as the whole and KIR^+ (KIR2D or KIR3DL1/DS1 positive) or KIR^- (KIR2D or KIR3DL1/DS1 negative) NK cell subsets were sorted into 5 µL of reverse transcription/pre-amplification mix, prior to multiplex qRT-PCR following manufacturer's protocol[48]. Briefly, the mix contained 2X Reaction mix and Superscript III (CellDirect One-Step qRT–PCR kit, Invitrogen) and 0,2X Taqman assay specific probes (Life technologies). Targeted cDNA pre-amplification was performed for 19 cycles and the pre-amplified product was diluted 1:5 in TE buffer before processing with Dynamic Array protocol according to the manufacturer's instructions (Fluidigm). All the probes used for this analysis are described in Supplementary Table 11. Mean expressions for *RPL27* and *GAPDH* house-keeping genes were used for signal normalization.

In vitro cell treatment and functional assay

PBMC were treated in cell culture medium (i.e., RPMI 1640 supplemented with 10% foetal bovine serum) with 0.5 µM or 1 µM of AZA, DAC, Dimethyloxaloylglycine (DMOG) (Sigma Aldrich), alone or in combination with 125µM Ascorbic Acid. Interleukin-2 (IL-2) (Miltenyi Biotec) was added to a final concentration of 100UI/mL. DMSO condition was used as control. The treatments were maintained for 5 days with a half change of medium after 48h (IL2 ± drugs or DMSO). Then, cells were collected and NK cells were analyzed for their phenotype (Supplementary Table 9 and Supplementary Fig. 9).

After treatment with DMOG, PBMCs were collected, enumerated and co-cultured with calcein-labelled K562 cells in 96-well U bottom plates in medium supplemented with Probenecid at 10:1 effector:target ratio. Killing was quantified after 4 hours of incubation at 37°C by measuring calcein-release into supernatant. Specific killing was calculated as below: (Measured fluorescence of K562+PBMC well – Spontaneous Fluorescence)/(Maximum fluorescence – Spontaneous fluorescence)*100.

For the *ex vivo* IFN-γ quantification, enriched NK cells from MDS patients enrolled in the NCT02985190 clinical trial[29] were cultured with PMA-Ionomycin (SIGMA, 50ng/mL and 500ng/mL respectively) for 5h

at 37°C. Brefeldin A (Sigma) was added at a final concentration of 10µg/ml after 1h of incubation. The percentage of IFN-γ positive cells was estimated by flow cytometry in the $CD3^{-}CD56^{+}$ NK cells. Spontaneous release was detected in the absence of target cells.

Statistical Analysis

Data are shown as median ± interquartile range, if not otherwise specified. Cytometry analysis were extracted from FlowJo v10.7 software and analyzed with Graph Pad Prism v8.0 software. Unpaired statistical analyses were calculated with the nonparametric Mann Whitney test. Paired statistics analyses were calculated with the nonparametric Wilcoxon matched pairs signed rank test. The Kolmogorov-Smirnov D test was used to calculate differences between treated/transfected and control situations. Pearson coefficient (r) was calculated to evaluate significant correlation. Receiver operation characteristic (ROC) curve was realized based on TET2 mutation status and percentage of KIR2D+ NK cells. Area under the curve, confidence interval, p-value and likelihood ratio were calculated. A Friedman test followed by a Dunn's test were used to calculate differences in experiments with multiple conditions. $p<0.05$ was considered as significant.

Data Availability

Reduced representation bisulfite sequencing (RRBS) data that support the findings of this study have been deposited in the Gene Expression Omnibus data repository with the accession number GSE183020 (http://www.ncbi.nlm.nih.gov/geo/query/acc.cgi?acc=GSE183020). The *in vitro* data generated in this study are available in the Supplementary information. Sequences of oligonucleotides used for the KIR genotyping (PCR-SSP) are limited to non-commercial and research use and are available upon request to Dr K. Gendzekhadze (kgendzek@coh.org), City Of Hope Medical Foundation, 1500 Duarte Rd, Duarte, CA 91010. Source data are provided with this paper as a Source Data file.

References

1. Ades L, Itzykson R, Fenaux P. Myelodysplastic syndromes. *Lancet* **383**, 2239-2252 (2014).
2. Gurion R*, et al.* 5-azacitidine prolongs overall survival in patients with myelodysplastic syndrome--a systematic review and meta-analysis. *Haematologica* **95**, 303-310 (2010).
3. Kantarjian H*, et al.* Decitabine improves patient outcomes in myelodysplastic syndromes: results of a phase III randomized study. *Cancer* **106**, 1794-1803 (2006).
4. Kunimoto H, Nakajima H. Epigenetic dysregulation of hematopoietic stem cells and preleukemic state. *Int J Hematol* **106**, 34-44 (2017).
5. Figueroa ME*, et al.* Leukemic IDH1 and IDH2 mutations result in a hypermethylation phenotype, disrupt TET2 function, and impair hematopoietic differentiation. *Cancer cell* **18**, 553-567 (2010).
6. Yamashita M, Dellorusso PV, Olson OC, Passegue E. Dysregulated haematopoietic stem cell behaviour in myeloid leukaemogenesis. *Nat Rev Cancer* **20**, 365-382 (2020).
7. Itzykson R*, et al.* Impact of TET2 mutations on response rate to azacitidine in myelodysplastic syndromes and low blast count acute myeloid leukemias. *Leukemia* **25**, 1147-1152 (2011).
8. Costantini B*, et al.* The effects of 5-azacytidine on the function and number of regulatory T cells and T-effectors in myelodysplastic syndrome. *Haematologica* **98**, 1196-1205 (2013).
9. Wang J, Xiao Z. Mesenchymal stem cells in pathogenesis of myelodysplastic syndromes. *Stem Cell Investig* **1**, 16 (2014).
10. Cooper MA, Fehniger TA, Caligiuri MA. The biology of human natural killer-cell subsets. *Trends Immunol* **22**, 633-640. (2001).

559 11. Morvan MG, Lanier LL. NK cells and cancer: you can teach innate cells new tricks. *Nat Rev Cancer* **16**,
560 7-19 (2016).

561 12. Epling-Burnette PK*, et al.* Reduced natural killer (NK) function associated with high-risk
562 myelodysplastic syndrome (MDS) and reduced expression of activating NK receptors. *Blood* **109**,
563 4816-4824 (2007).

564 13. Khaznadar Z*, et al.* Defective NK Cells in Acute Myeloid Leukemia Patients at Diagnosis Are
565 Associated with Blast Transcriptional Signatures of Immune Evasion. *J Immunol* **195**, 2580-2590
566 (2015).

567 14. Costello RT*, et al.* Defective expression and function of natural killer cell-triggering receptors in
568 patients with acute myeloid leukemia. *Blood* **99**, 3661-3667 (2002).

569 15. Kiladjian JJ*, et al.* Cytolytic function and survival of natural killer cells are severely altered in
570 myelodysplastic syndromes. *Leukemia* **20**, 463-470 (2006).

571 16. Bjorkstrom NK*, et al.* Expression patterns of NKG2A, KIR, and CD57 define a process of CD56dim NK-
572 cell differentiation uncoupled from NK-cell education. *Blood* **116**, 3853-3864 (2010).

573 17. Amorim LM*, et al.* High-Resolution Characterization of KIR Genes in a Large North American Cohort
574 Reveals Novel Details of Structural and Sequence Diversity. *Front Immunol* **12**, 674778 (2021).

575 18. Tate JG*, et al.* COSMIC: the Catalogue Of Somatic Mutations In Cancer. *Nucleic Acids Res* **47**, D941-
576 D947 (2019).

577 19. Shihab HA*, et al.* An integrative approach to predicting the functional effects of non-coding and
578 coding sequence variation. *Bioinformatics* **31**, 1536-1543 (2015).

20. Zhang D, An X, Li Z, Zhang S. Role of gene promoter methylation regulated by TETs and DNMTs in the overexpression of HLA-G in MCF-7 cells. *Experimental and therapeutic medicine* **17**, 4709-4714 (2019).

21. An integrated encyclopedia of DNA elements in the human genome. *Nature* **489**, 57-74 (2012).

22. Wu CY, Zhang B, Kim H, Anderson SK, Miller JS, Cichocki F. Ascorbic Acid Promotes KIR Demethylation during Early NK Cell Differentiation. *The Journal of Immunology* **205**, 1513-1523 (2020).

23. Minor EA, Court BL, Young JI, Wang G. Ascorbate induces ten-eleven translocation (Tet) methylcytosine dioxygenase-mediated generation of 5-hydroxymethylcytosine. *J Biol Chem* **288**, 13669-13674 (2013).

24. Rasmussen KD*, et al.* Loss of TET2 in hematopoietic cells leads to DNA hypermethylation of active enhancers and induction of leukemogenesis. *Genes Dev* **29**, 910-922 (2015).

25. Kanehisa M, Goto S. KEGG: kyoto encyclopedia of genes and genomes. *Nucleic Acids Res* **28**, 27-30 (2000).

26. Nakauchi Y*, et al.* The Cell Type-Specific 5hmC Landscape and Dynamics of Healthy Human Hematopoiesis and TET2-Mutant Preleukemia. *Blood cancer discovery* **3**, 346-367 (2022).

27. Tulstrup M*, et al.* TET2 mutations are associated with hypermethylation at key regulatory enhancers in normal and malignant hematopoiesis. *Nat Commun* **12**, 6061 (2021).

28. Dulphy N*, et al.* Underground Adaptation to a Hostile Environment: Acute Myeloid Leukemia vs. Natural Killer Cells. *Front Immunol* **7**, 94 (2016).

29. Mekinian A*, et al.* A Phase II prospective trial of azacitidine in steroid-dependent or refractory systemic autoimmune/inflammatory disorders and VEXAS syndrome associated with MDS and CMML. *Leukemia*, (2022).

30. Carlsten M*, et al.* Reduced DNAM-1 expression on bone marrow NK cells associated with impaired killing of CD34+ blasts in myelodysplastic syndrome. *Leukemia* **24**, 1607-1616 (2010).

31. Stringaris K*, et al.* KIR gene haplotype: an independent predictor of clinical outcome in MDS patients. *Blood* **128**, 2819-2823 (2016).

32. Lio CJ, Yuita H, Rao A. Dysregulation of the TET family of epigenetic regulators in lymphoid and myeloid malignancies. *Blood* **134**, 1487-1497 (2019).

33. Pastoret C*, et al.* Linking the KIR phenotype with STAT3 and TET2 mutations to identify chronic lymphoproliferative disorders of NK cells. *Blood* **137**, 3237-3250 (2021).

34. Olson TL*, et al.* Frequent somatic TET2 mutations in chronic NK-LGL leukemia with distinct patterns of cytopenias. *Blood* **138**, 662-673 (2021).

35. Kaasinen E*, et al.* Impact of constitutional TET2 haploinsufficiency on molecular and clinical phenotype in humans. *Nat Commun* **10**, 1252 (2019).

36. Stremenova Spegarova J*, et al.* Germline TET2 loss of function causes childhood immunodeficiency and lymphoma. *Blood* **136**, 1055-1066 (2020).

37. Steensma DP*, et al.* Clonal hematopoiesis of indeterminate potential and its distinction from myelodysplastic syndromes. *Blood* **126**, 9-16 (2015).

38. Arends CM*, et al.* Hematopoietic lineage distribution and evolutionary dynamics of clonal hematopoiesis. *Leukemia* **32**, 1908-1919 (2018).

39. Hong M, He G. The 2016 Revision to the World Health Organization Classification of Myelodysplastic Syndromes. *J Transl Int Med* **5**, 139-143 (2017).

40. Greenberg PL*, et al.* Revised international prognostic scoring system for myelodysplastic syndromes. *Blood* **120**, 2454-2465 (2012).

41. Cheson BD*, et al.* Clinical application and proposal for modification of the International Working Group (IWG) response criteria in myelodysplasia. *Blood* **108**, 419-425 (2006).

42. Sun JY*, et al.* Development of a multiplex PCR-SSP method for Killer-cell immunoglobulin-like receptor genotyping. *Tissue Antigens* **64**, 462-468 (2004).

43. Cooley S*, et al.* Donor selection for natural killer cell receptor genes leads to superior survival after unrelated transplantation for acute myelogenous leukemia. *Blood* **116**, 2411-2419 (2010).

44. Zhou X*, et al.* Exploring genomic alteration in pediatric cancer using ProteinPaint. *Nat Genet* **48**, 4-6 (2016).

45. Hu L*, et al.* Crystal structure of TET2-DNA complex: insight into TET-mediated 5mC oxidation. *Cell* **155**, 1545-1555 (2013).

46. Longo PA, Kavran JM, Kim MS, Leahy DJ. Single cell cloning of a stable mammalian cell line. *Methods in enzymology* **536**, 165-172 (2014).

47. Cimmino L*, et al.* Restoration of TET2 Function Blocks Aberrant Self-Renewal and Leukemia Progression. *Cell* **170**, 1079-1095 e1020 (2017).

48. Thai LH*, et al.* BAFF and CD4(+) T cells are major survival factors for long-lived splenic plasma cells in a B-cell-depletion context. *Blood* **131**, 1545-1555 (2018).

Acknowledgments

This study was supported by a grant from the French Ministry of Health and the French National Cancer Institute (#PRT-K2017-109), the Cancéropôle Ile-de-France, the Association Laurette Fugain (#ALF 2016-07), the Association Force Hémato (Call for projects 2017), the Ligue contre le Cancer (Ile-de-France committee), the Association Saint-Louis pour la Recherche sur les Leucémies, and the Association pour la Recherche en Immunologie Médicale et Expérimentale (ARIME). The authors want to acknowledge the support by the "Groupe Francophone des Myelodysplasies (GFM)" in the management of the NCT02985190 clinical trial. The authors thank Niclas Setterblad, Christelle Doliger, Sophie Duchez from the IRSL's Technological Platform, Nolwenn Legrand from the EFS laboratory in Nantes, as well as Pierre De La Grange and Wail Zeitouni from Genosplice for their technical and analytic support.

Author contributions

M.B., V.B. and N.D. designed, analyzed and interpreted all experiments, and wrote the manuscript. M.B. V.B., F.G., and E.L. performed experiments and analyzed the data. L-P.Z. managed the collection of the patients' samples and clinical information. B.S. analyzed the RRBS data. G.H. and J.V. performed preliminary feasibility experiments. F. R-L. provided reagents and analyzed data. K.G. and C.R. performed KIR genotyping. L.L., R.K. and E.C. performed next-generation sequencing and analyzed mutation profile data. L-P.Z., M.S., P.F and L.A. recruited the patients for the study. A.M., O.F. and P.F. supervised the NCT02985190 clinical trial. A.C, M.E., K.B., A.T., P.F. and L.A. contributed to the scientific orientation of the study and critically reviewed the manuscript. L.A. designed the patients' cohort suitable for the study. N.D. supervised the study.

Competing interests

The authors declare no competing interests.

Materials & Correspondence

664 Correspondence and material requests should be addressed to:

665 Dr Nicolas DULPHY

666 INSERM UMR_S1160, Institut de Recherche Saint Louis, Hopital Saint-Louis, 1 avenue Claude

667 Vellefaux, F-75010 Paris, France

668 Email: nicolas.dulphy@u-paris.fr

Figures

Fig. 1: *TET2/IDH* mutations in MDS/CMML patients lead to the reduction of KIR and Perforin expression in NK cells.

(a) Percentages of blood NK cells expressing activating (NKp30, NKp46, DNAM-1, NKG2D) and inhibitory (CD96, CD85j, KIR2D, NKG2A) receptors, and maturation/activation markers (KLRG1, CD69, CD57) were measured by flow cytometry in *TET2/IDH*^{WT} (n=13, n=11 for NKG2A) and *TET2/IDH*^{MUT} (n=19, n=15 for NKG2A) MDS/CMML patients. Statistics were calculated with the nonparametric Mann-Whitney test, two-sided, KIR2D *** p=0.0005, NKG2A * p= 0.0246. **(b)** Percentages of KIR2D^{+} BM NK cells measured by flow cytometry in *TET2/IDH*^{WT} (n=12) and *TET2/IDH*^{MUT} (n=7) MDS/CMML patients. Statistics were calculated with the nonparametric Mann-Whitney test two sided * p=0.013. **(c-d)** Specific expression of KIR2DL1, KIR2DL2/DL3 and KIR3DL1/DL2 in blood NK cells detected by flow cytometry in *TET2/IDH*^{WT} (n=11) and *TET2/IDH*^{MUT} (n=15) MDS/CMML patients. One representative example is shown in (C). Statistics were calculated with the nonparametric Mann-Whitney test, KIR2DL1 ** p=0.0092, two sided KIR2DL2/DL3 ** p= 0.0077. **(e)** Intracellular perforin and granzyme B expression in blood NK cells measured by flow cytometry in *TET2/IDH*^{WT} (n=19) and *TET2/IDH*^{MUT} (n=22) MDS/CMML patients. Statistics were calculated with the nonparametric Mann-Whitney test * p=0.0337 **(f)** Receiver operating characteristic (ROC) curve depicting the relationship of true *TET2* mutation presence (sensitivity) and false *TET2* mutation presence (100%-specificity) for a KIR2D expression threshold at 25% in blood NK cells (p<0.0001) quantified by flow cytometry in *TET2/IDH*^{WT} (n=19) and *TET2*^{MUT} (n=17) MDS/CMML patients. **(g)** KIR2D expression on blood NK cells of the *TET2/IDH*^{WT} (n=19), *TET2*^{MUT} (n=17) and *IDH*^{MUT} (n=5) patients showed in the ROC curve. The horizontal black bar indicates the threshold at 25% KIR2D^{+} NK cells. Statistics were calculated with the nonparametric Mann-Whitney test, *TET2/IDH*^{WT} vs *TET2*^{MUT}: **** p<0.0001; *TET2/IDH*^{WT} vs *IDH*^{MUT}: * p=0.0152. For all the analysis, data are presented as medians and interquartile ranges. Source data are provided as a Source Data file.

Fig. 2: *TET2* mutations identified in bulk cells of MDS patients at diagnosis are also observed in NK cells and correlate with KIR2D expression.

(a) The percentage of Variant Allele Frequency (VAF) for the mutations of *TET2* observed in the white mononuclear cells (WMC) and in sorted NK/T cells at diagnosis of $TET2^{MUT}$ MDS/CMML patients (n=10) was evaluated by NGS analysis (with a range from 1 to 4 mutations per patient). Data are represented as box-and-whisker plot (minimum VAF, 25% percentile, median, 75% percentile and maximum VAF respectively for WMC: 0%, 11.25%, 32.5%, 42.5%, 49%; for NK cells: 0%, 3.5%, 14%, 35.5%, 54%; and for T cells: 0%, 0%, 0%, 0%, 7%). Nonparametric two-sided Wilcoxon matched pairs signed rank test was used to determine statistical significance. **** $p<0.0001$ **(b)** VAF (%) of the different mutations detected in the WMC at diagnosis (blue) and in sorted NK cells (red) in 4 patients (MUT08, MUT22, MUT19, MUT31; see **Supplementary Table 6** for more information). **(c)** Correlation curve between the percentage of $KIR2D^{+}$ NK cells and the *TET2* VAF (%) in blood NK cells from the MDS/CMML patients analyzed in (A). Linear regression was calculated, $r=0.88$, $p<0.0001$. **(d)** The VAF percentage in the WMC and in sorted KIR+ and KIR- NK cells at diagnosis from $TET2^{MUT}$ MDS/CMML patients (n=5, range from 1 to 4 mutations per patient) was evaluated by NGS analysis. Data are represented as box-and-whisker plot (minimum VAF, 25% percentile, median, 75% percentile and maximum VAF respectively for KIR- NK cells: 6.1%, 8.3%, 18.2%, 36.5%, 42.1%; and KIR+ NK cells: 0%, 1.2%, 7.3%, 13%, 48%). Statistics were calculated with two-sided nonparametric Wilcoxon matched pairs signed rank test. * $p=0.0186$. Source data are provided as a Source Data file.

Fig. 3: TET2 regulates KIR expression on NK cells through its binding onto and regulating methylation of the KIR locus.

(a) *TET2* mutational landscape in the 13 *TET2*^{MUT}patients with KIR2D expression below 25% established with the St Jude protein paint software (https://proteinpaint.stjude.org/). Mutations were classified as Missense (blue), Frameshift (red) and Nonsense (orange). Numbers associated to each mutation designed patients (**Supplementary Data 1**). **(b)** Percentage of KIR2D^{+} NK cells after 5 days of *in vitro* treatment with 1µM DMOG (n=10). DMSO alone was used as control. One dot represents one PBMC sample. Nonparametric two-sided Wilcoxon matched pairs signed rank test was used to determine statistical significance. **p= 0.0059. Data are presented as median and interquartile range . **(c)** Fold enrichment of sequences specific for the Cis-regulatory element (CRE), *KIR2DL1* promoter and *KIR2DL2/3* promoter analyzed in sorted NK cells by ChIP-qPCR with TET2, H3 or H3K18 specific mAbs or IgG istotype control. Means ± SD are shown (n=3). Each dot represents one independent experiment. **(d)** Luciferase activity in HEK293T cells co-transfected with a *TET2* full length plasmid or an empty plasmid as control, and the luciferase-reporter construct containing the region (-147+60) of the *KIR2DL1* promoter. Means ± SD are shown (n=4). Each dot represents one independent experiment. Nonparametric two-sided Wilcoxon matched-pairs signed rank test was used to determine statistical significance. *p= 0.0286 **(e)** Jurkat cells transfected with the *KIR2DL1* promoter-luciferase reporter plasmid were treated with 500µM of L-AA for 16h and analyzed by detecting luminescence signal. Means ± SD are shown (n=4). Each dot represents one independent experiment. Nonparametric two-sided Wilcoxon matched pairs signed rank test was used to determine statistical significance. *p= 0.0286 **(f)** RRBS DNA methylation profiles of the extended KIR locus of NK cells with low or high KIR2D expression. Each graph represents the DNA methylation profile of sorted NK cells from blood samples of 5 patients; vertical bars represent the percentage of DNA methylation at CpG position. CRE and *KIR* genes were highlighted in green and grey respectively. **(g-h)** IGV (Integrative Genomics Viewer) view of CpG read signals corresponding to DNA methylation in NK cell, based on the high (*TET2*$^{WT/MUT}$KIR^{HIGH}, in blue bars) and low (*TET2*^{MUT}KIR^{LOW}, in red bars) KIR expression. Genome profiles at the CRE region **(g)** and the *KIR2DL1* gene **(h)** loci

742 showed variation in the DNA methylation pattern between the two groups of patient NK cells. Red
743 peaks/boxes show significant differences in the DNA methylation levels at particular CpG positions of
744 these specific loci. Source data are provided as a Source Data file.
745

Fig. 4: Loss of TET2 leads to DNA hypermethylation and decrease key gene expression for NK cells function.

(a) Circos plots showing whole-genome CpG methylation status in patient MUT14 characterised by the absence of *TET2* mutations in NK cells and a high expression of KIR2D, and in patient MUT22 with a VAF of 50% for the *TET2* mutation [NM_001127208:exon11:c,4669_4672del:p.V1557fs] and a very low expression of KIR2D in NK cells. **(b)** Volcano plots and heatmaps showed the overall increase of global DNA methylation levels reported after RRBS analysis, in the *TET2*^{MUT}KIR^{LOW} (n=3) *vs.* *TET2*$^{WT/MUT}$KIR^{HIGH} (n=2) NK cells. Heatmaps depicted supervised clustering of the significantly modified sited and genes between patients' subgroups. Blue dots/bars show the hypomethylated CpG/genes whereas red dots/bars show the hypermethylated ones (methylation difference ≥ 20%, unadjusted p-value ≤ 0.05). Top panel shows the differentially methylated CpG sites. Bottom panel shows the differentially methylated genes. **(c)** GO-enrichment analysis on the differentially methylated genes in the *TET2*^{MUT}KIR^{LOW} and *TET2*$^{WT/MUT}$KIR^{HIGH} NK cells. Percentages of methylated CpG sites were calculated in gene bodies and 10kb upstream or downstream of the gene of interest in *TET2*^{MUT}KIR^{LOW} and *TET2*$^{WT/MUT}$KIR^{HIGH} NK cells (in red and blue respectively) and aggregated across all genes of a given KEGG pathway for each sample. Pathways of interest shown are the cytokine-cytokine receptor interactions (KEGG reference hsa04060), the JAK-STAT signalling pathway (hsa04630), the TNF signalling pathway (hsa04668) and the NK cell mediated cytotoxicity pathway (hsa04650). Source data are provided as a Source Data file.

Fig. 5: Hypermethylation of particular CpG sites repress NK cell genes expression and function. **(a)** Methylation profiles, established after RRBS analyses, depicted with IVG at the *IFNG* (upper panel), *TNF* (middle panel) and *PRF1* (lower panel) loci, were shown in NK cells from patients segregated on the high (*TET2*$^{WT/MUT}$KIR^{HIGH}, in blue bars) and low (*TET2*^{MUT}KIR^{LOW}, in red bars) KIR expression. Red peaks/boxes show significant differences in the DNA methylation levels of these specific loci. **(b)** The regulatory activity of specific CpG sites was analysed in the HEK293T cell line transfected with a luciferase-reporter plasmid including methylated or non-methylated genes' regulatory regions. Relative luciferase activities of the *in vitro* methylated regions were compared to their non-methylated counterpart (FC= Methylated/Putative Promoter). Means ± SD are shown (n=4). Data were analysed using the one-way Friedman test followed by a Dunn's test. *p=0.0433 **(c)** Quantification of the *KIR2DL1*, *TNF* and *IFNG* transcripts by RT-qPCR on KIR2D^{-} NK cells sorted from *TET2/IDH*^{WT} (n=11, in blue) and *TET2*^{MUT} (n=10, in red) patients. Medians and interquartiles are shown. Statistics were calculated with the two-sided Mann-Whitney test, **p=0.0036. **(d)** Fold changes of NK cells killing activity against the NK-sensitive cell line K562 previously treated for 5 days with 1µM DMOG (n=10). Each dot represents one independent experiment. DMSO alone was used as control. Means ± SD are shown. Data were analysed using the one-way Friedman test followed by a Dunn's test. *p=0.0417. Source data are provided as a Source Data file.

Fig. 6: Hypomethylating agents normalize the NK cell phenotype of MDS patients.

(a) Evaluation of KIR2D surface expression on NK cells of *TET2/IDH*^{MUT} patients after treatment with azacitidine (AZA, n=12), decitabine (DAC, n=12), acid ascorbic (AA, n=7), and DAC+AA (n=7). Nonparametric two-sided Wilcoxon matched pairs signed rank test was used to determine statistical significance, DAC: *** p=0.001, DAC+AA: * p=0.0156. **(b)** NK cells were isolated from patients PBMC before and after 3 cycles of treatment with AZA, and cultured overnight at 100U/ml of IL-2. Subsequently cells were cultured with PMA-Ionomycin for 6h. The frequency of responding cells in terms of IFN-γ were assessed by flow cytometry (n=7). **(c)** KIR2D, perforin and granzyme B expression was measured by flow cytometry in blood of MDS patients (n=9) before (in blue) and after (in red) 6 cycles of AZA treatment. Nonparametric two-sided Wilcoxon matched pairs signed rank test was used to determine statistical significance, KIR2D: * p=0.0195, Perforin: * p=0.0273, Granzyme B: * p=0.0273. Data are presented as medians and interquartile ranges. Source data are provided as a Source Data file.

figure 1

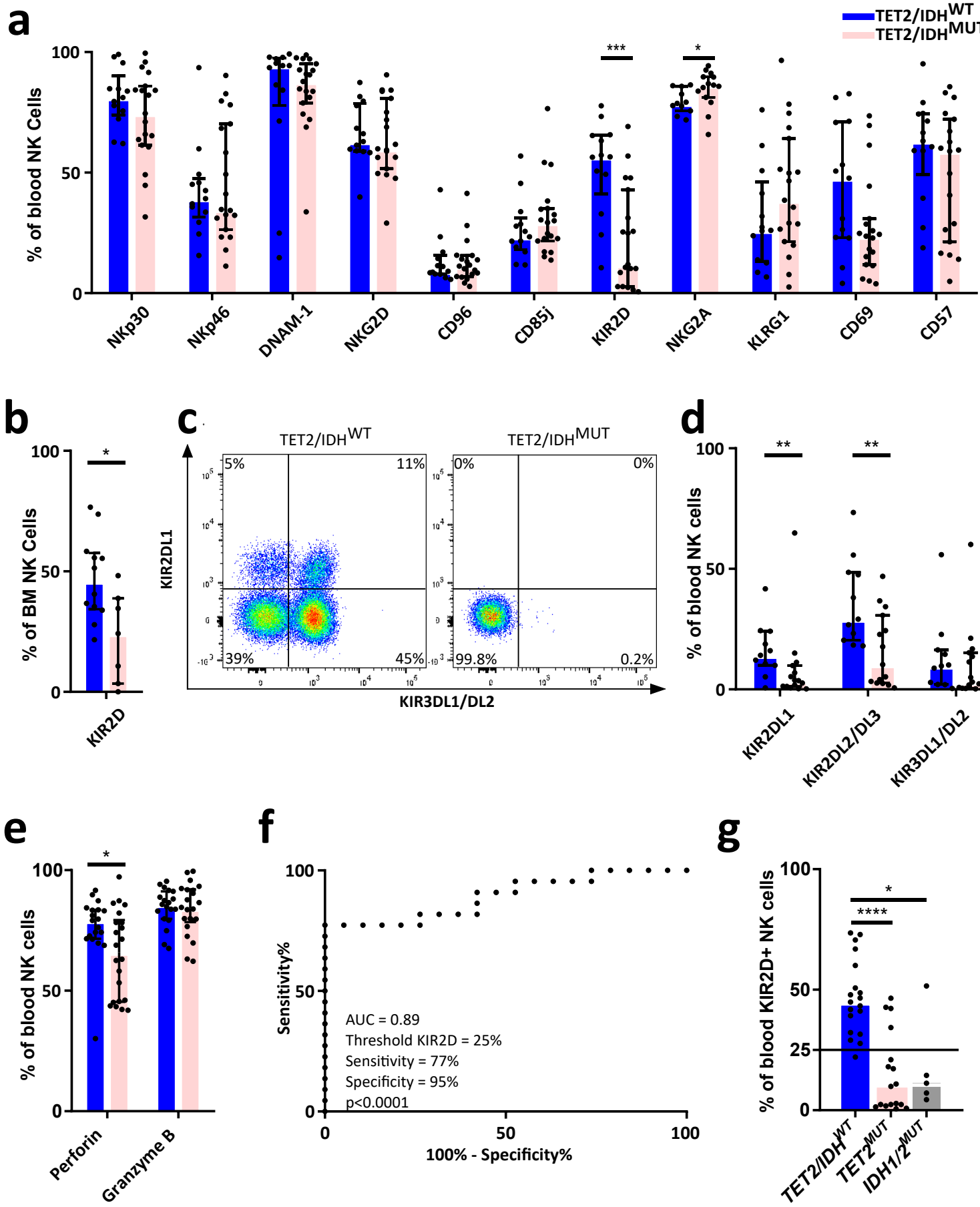
a
TET2/IDH^WT
TET2/IDH^MUT
% of blood NK Cells
NKp30
NKp46
DNAM-1
NKG2D
CD96
CD85j
KIR2D
NKG2A
KLRG1
CD69
CD57
b
% of BM NK Cells
KIR2D
c
TET2/IDH^WT
TET2/IDH^MUT
KIR2DL1
KIR3DL1/DL2
5%
11%
39%
45%
0%
0%
99.8%
0.2%
d
% of blood NK cells
KIR2DL1
KIR2DL2/DL3
KIR3DL1/DL2
e
% of blood NK cells
Perforin
Granzyme B
f
Sensitivity%
100% - Specificity%
AUC = 0.89
Threshold KIR2D = 25%
Sensitivity = 77%
Specificity = 95%
p<0.0001
g
% of blood KIR2D+ NK cells
TET2/IDH^WT
TET2^MUT
IDH1/2^MUT

figure 2

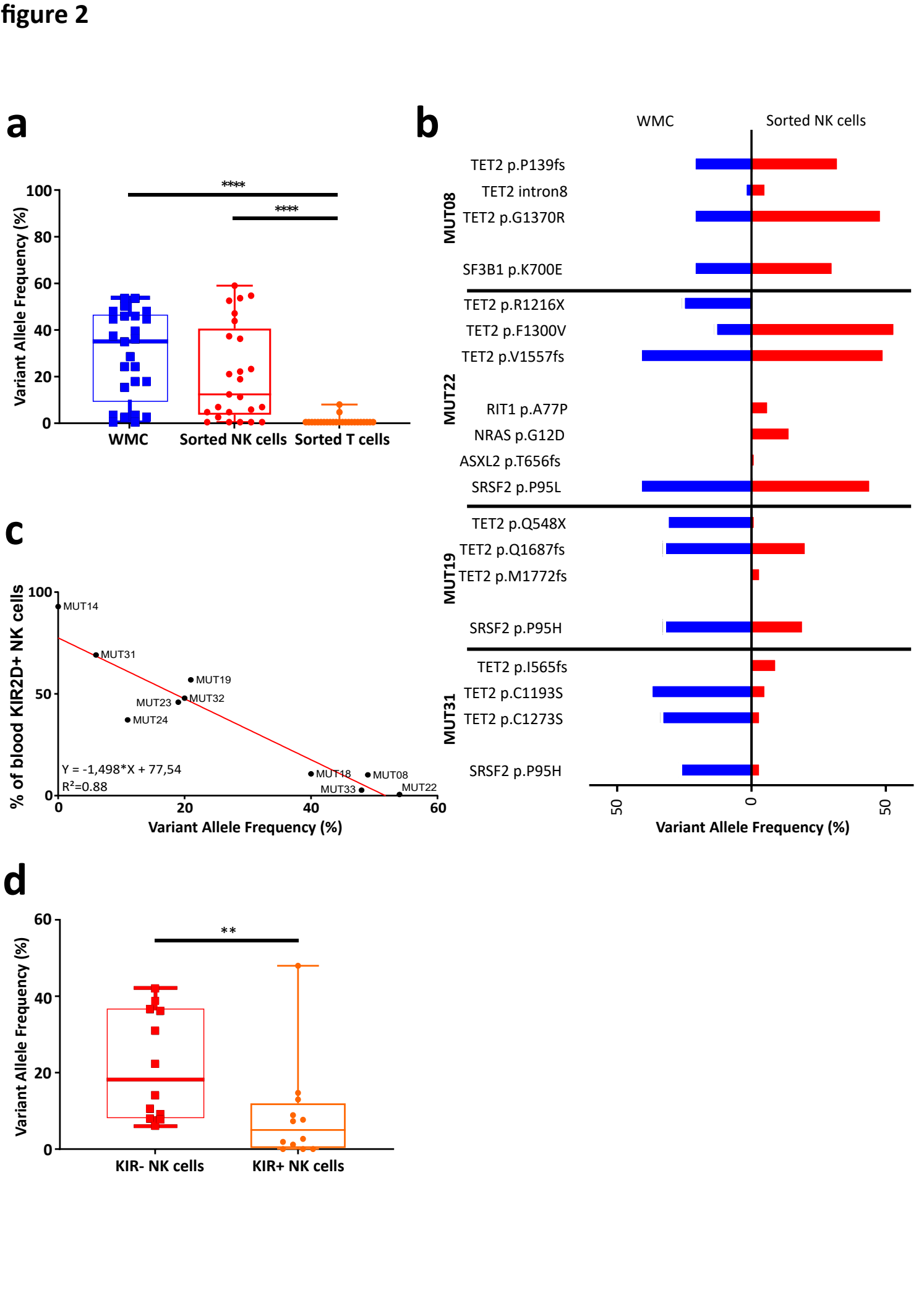
a
Variant Allele Frequency (%)
****
****
WMC
Sorted NK cells
Sorted T cells
b
WMC
Sorted NK cells
MUT08
TET2 p.P139fs
TET2 intron8
TET2 p.G1370R
SF3B1 p.K700E
MUT22
TET2 p.R1216X
TET2 p.F1300V
TET2 p.V1557fs
RIT1 p.A77P
NRAS p.G12D
ASXL2 p.T656fs
SRSF2 p.P95L
MUT19
TET2 p.Q548X
TET2 p.Q1687fs
TET2 p.M1772fs
SRSF2 p.P95H
MUT31
TET2 p.I565fs
TET2 p.C1193S
TET2 p.C1273S
SRSF2 p.P95H
Variant Allele Frequency (%)
c
% of blood KIR2D+ NK cells
MUT14
MUT31
MUT19
MUT23
MUT32
MUT24
MUT18
MUT08
MUT33
MUT22
Y = -1,498*X + 77,54
R²=0.88
Variant Allele Frequency (%)
d
Variant Allele Frequency (%)
**
KIR- NK cells
KIR+ NK cells

figure 3

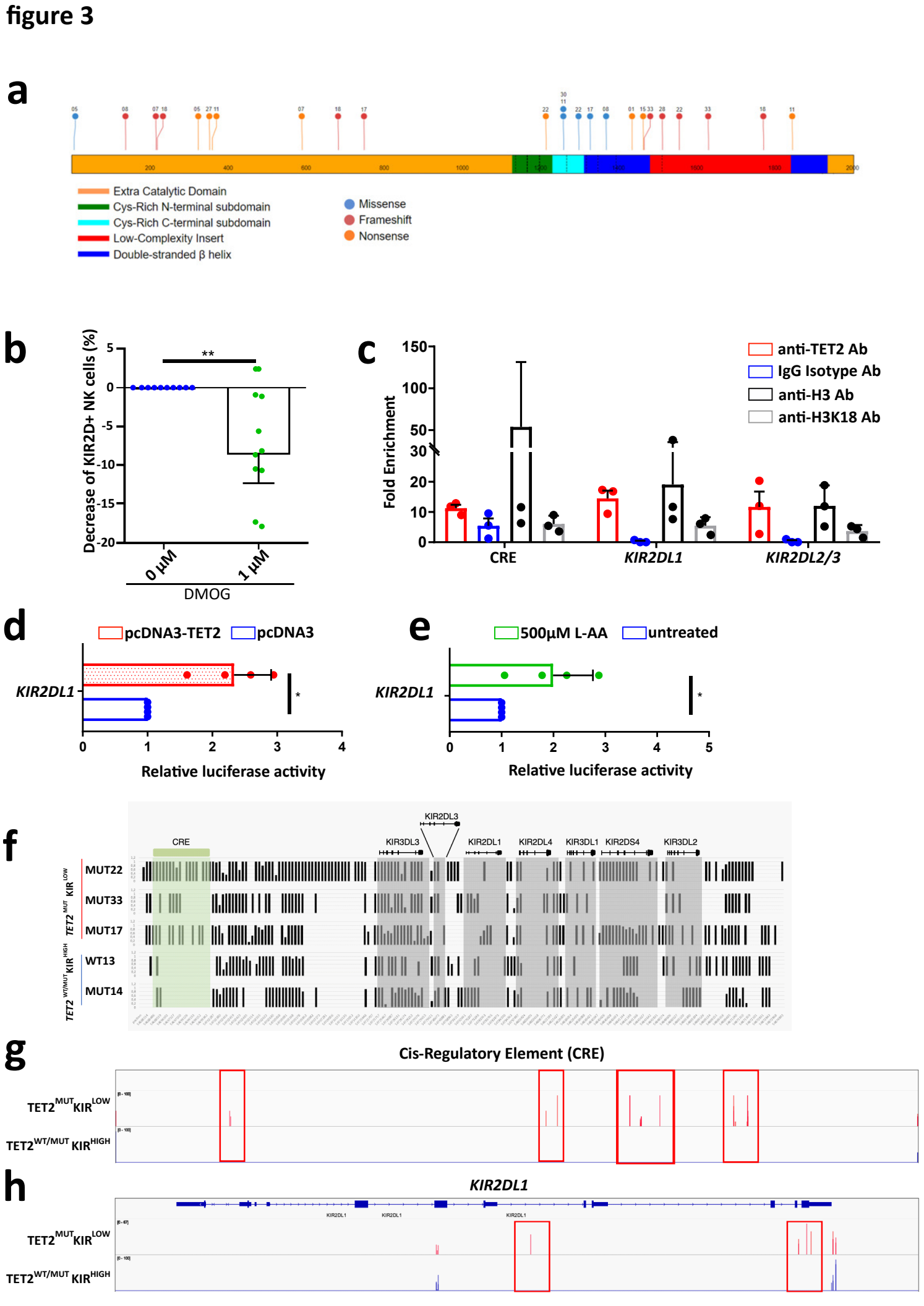
a
Extra Catalytic Domain
Cys-Rich N-terminal subdomain
Cys-Rich C-terminal subdomain
Low-Complexity Insert
Double-stranded β helix
Missense
Frameshift
Nonsense
b
Decrease of KIR2D+ NK cells (%)
**
0 μM
1 μM
DMOG
c
Fold Enrichment
anti-TET2 Ab
IgG Isotype Ab
anti-H3 Ab
anti-H3K18 Ab
CRE
KIR2DL1
KIR2DL2/3
d
pcDNA3-TET2
pcDNA3
KIR2DL1
Relative luciferase activity
e
500μM L-AA
untreated
KIR2DL1
Relative luciferase activity
f
CRE
KIR2DL3
KIR3DL3
KIR2DL1
KIR2DL4
KIR3DL1
KIR2DS4
KIR3DL2
MUT22
MUT33
MUT17
WT13
MUT14
TET2MUT KIRLOW
TET2WT/MUT KIRHIGH
g
Cis-Regulatory Element (CRE)
TET2MUT KIRLOW
TET2WT/MUT KIRHIGH
h
KIR2DL1
TET2MUT KIRLOW
TET2WT/MUT KIRHIGH

figure 4

a

TET2 VAF in NK 0%
CpG Methylation 45.6 %
KIR2D 90 %

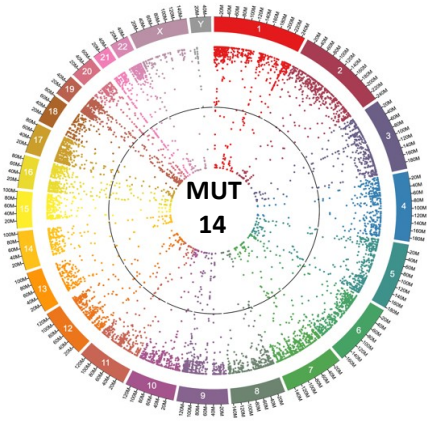

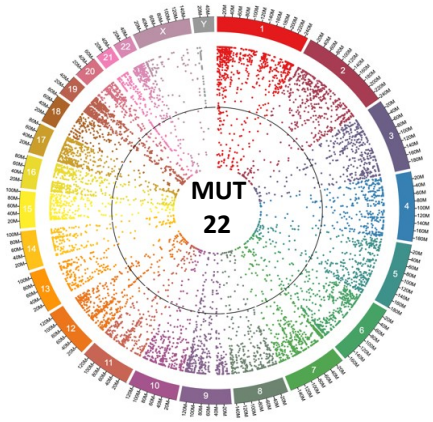

TET2 VAF in NK 50%
CpG Methylation 51.9 %
KIR2D 0.58 %

b

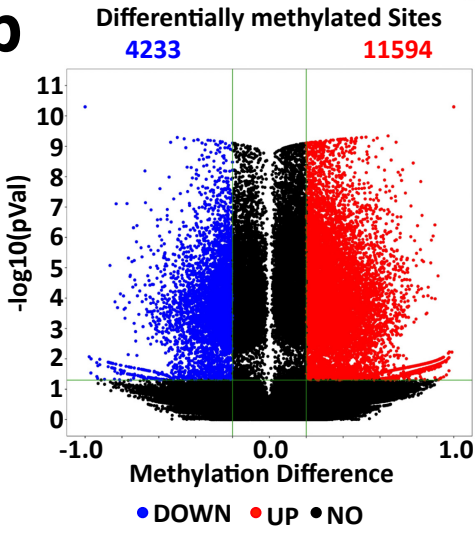

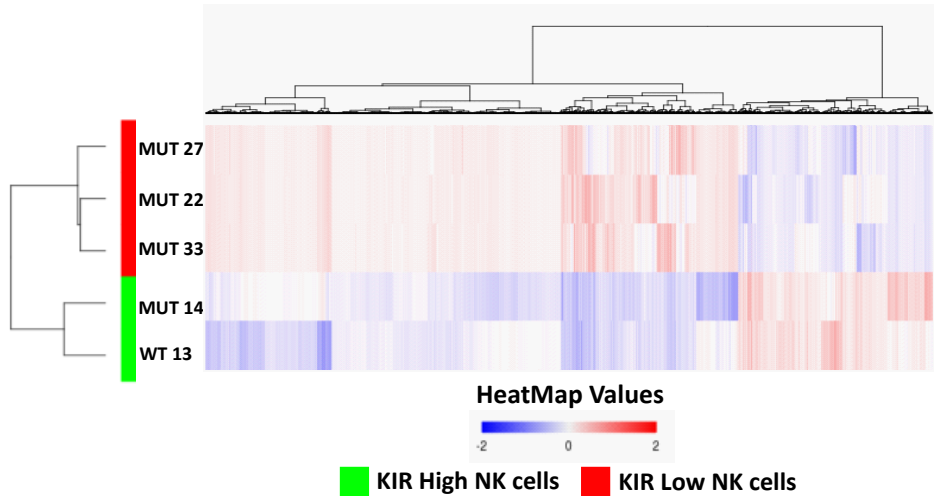

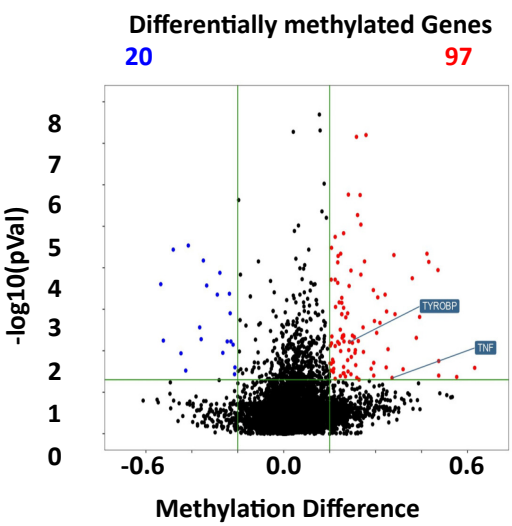

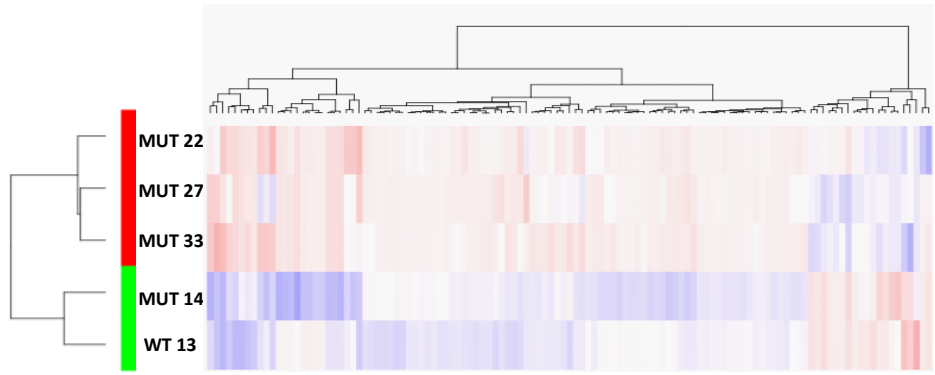

c

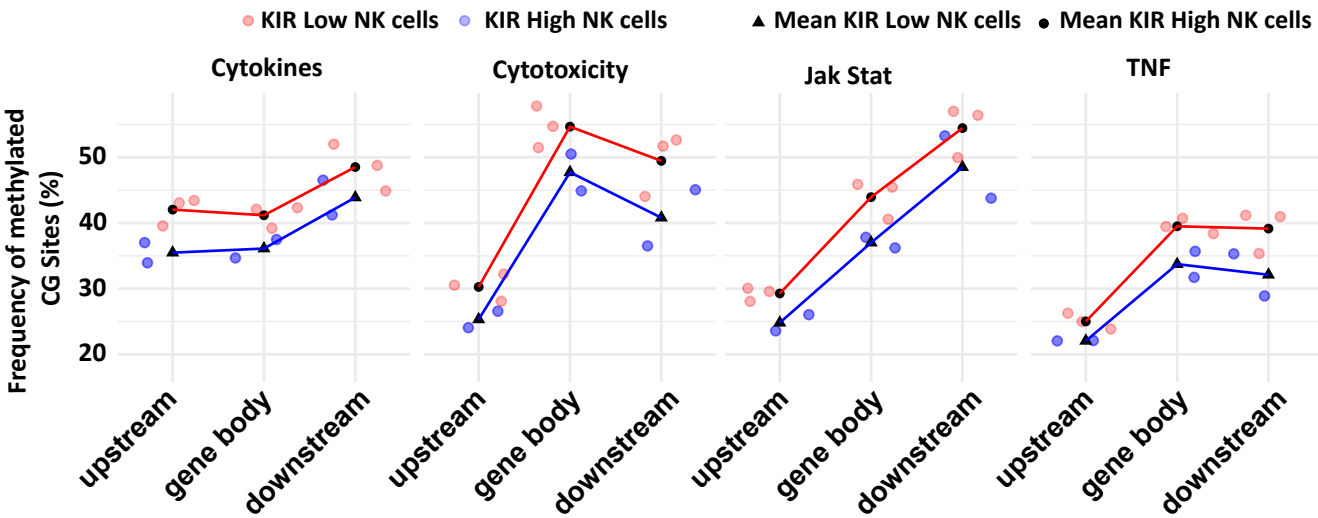

figure 5

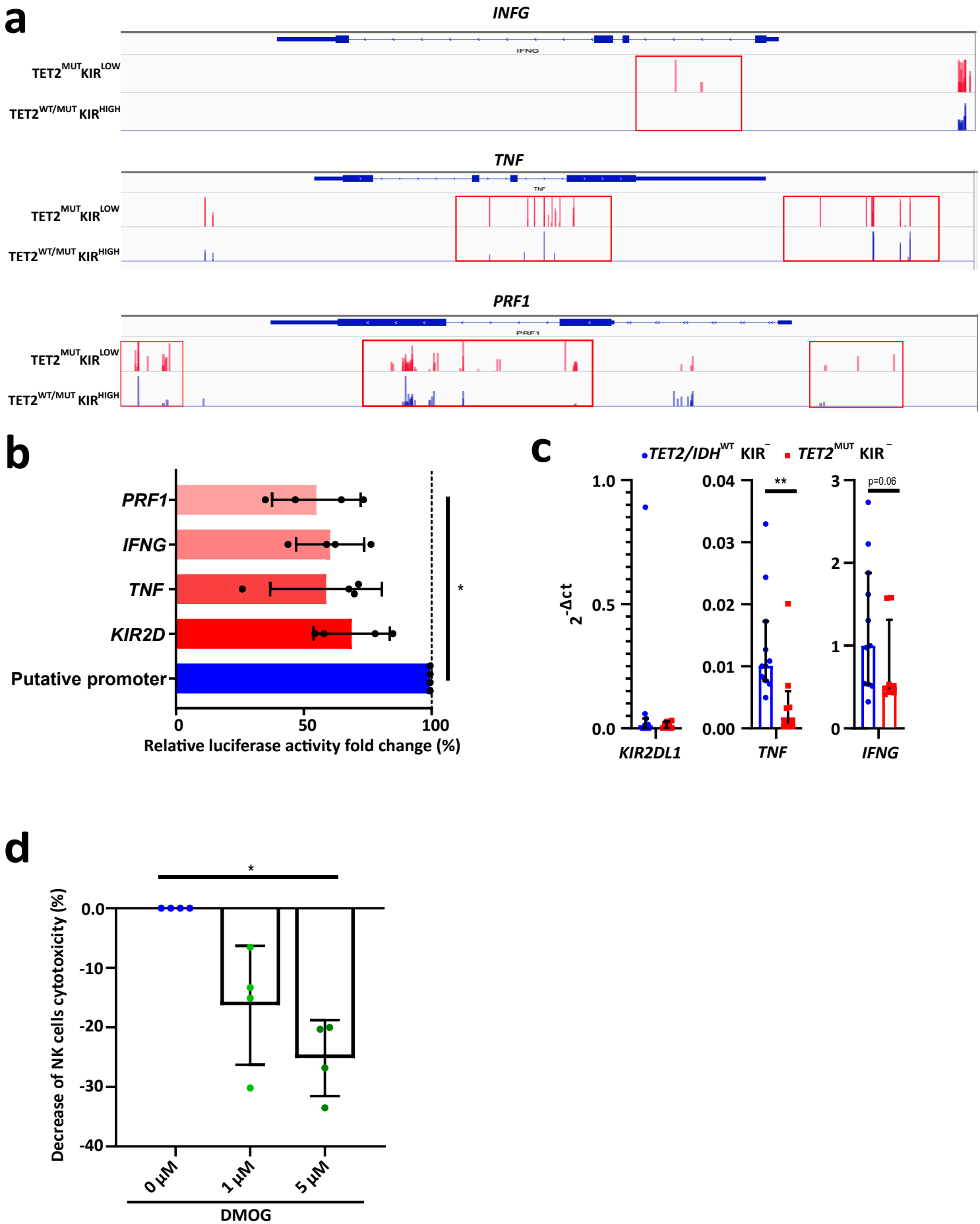
a
INFG
IFNG
TET2MUT KIRLOW
TET2WT/MUT KIRHIGH
TNF
TNF
TET2MUT KIRLOW
TET2WT/MUT KIRHIGH
PRF1
PRF1
TET2MUT KIRLOW
TET2WT/MUT KIRHIGH
b
PRF1
IFNG
TNF
KIR2D
Putative promoter
*
0
50
100
Relative luciferase activity fold change (%)
c
TET2/IDHWT KIR−
TET2MUT KIR−
1.0
0.5
0.0
2-Δct
KIR2DL1
0.04
0.03
0.02
0.01
0.00
**
TNF
3
2
1
0
p=0.06
IFNG
d
*
0.0
-10
-20
-30
-40
Decrease of NK cells cytotoxicity (%)
0 µM
1 µM
5 µM
DMOG

figure 6

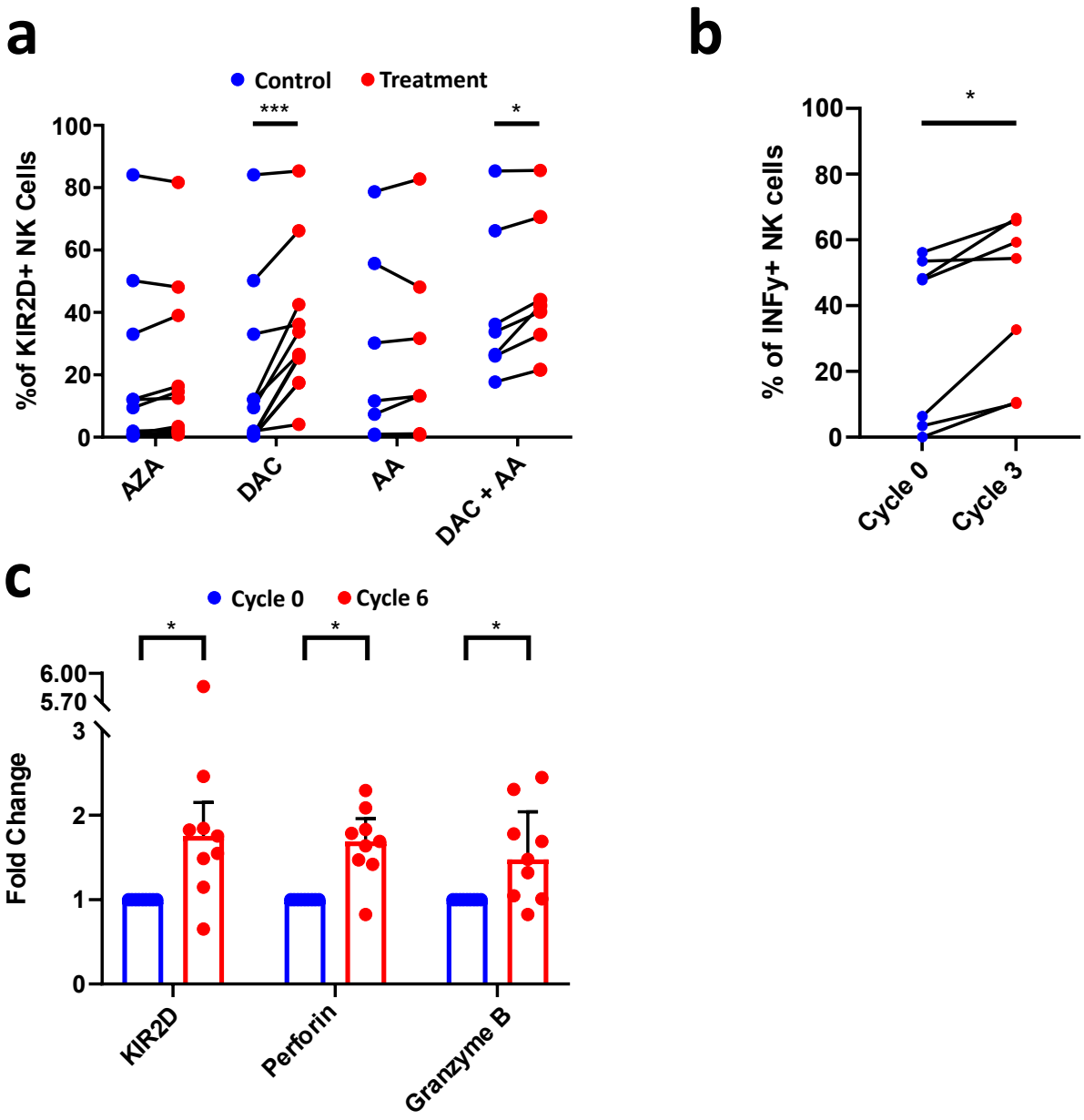
a
Control
Treatment
***
*
%of KIR2D+ NK Cells
100
80
60
40
20
0
AZA
DAC
AA
DAC + AA
b
*
% of INFy+ NK cells
100
80
60
40
20
0
Cycle 0
Cycle 3
c
Cycle 0
Cycle 6
*
*
*
Fold Change
6.00
5.70
3
2
1
0
KIR2D
Perforin
Granzyme B